Similitude of Hypersonic Flows Over Slender Bodies in Nonequilibrium Dissociated Gases[1]

GEORGE R. INGER[2]
Aerospace Corporation, El Segundo, Calif.

This paper is concerned with the similitude laws governing inviscid, nonequilibrium gas flows around blunt or sharp-nosed slender bodies at zero angle of attack, based on the hypersonic small disturbance flow theory. Some related features of the interaction between the effects of nose bluntness and nonequilibrium dissociation and vibration and the influence of a dissociated freestream are also discussed. The hypersonic equivalence principle and the related similitude for affinely related bodies are set forth for nonequilibrium flows in either diatomic gases or a gas mixture such as air. For a family of diatomic gases, as opposed to a given gas such as air, a generalized ambient gas state scaling condition is obtained, whereby the ambient density and temperature need not be simulated. A detailed discussion is given of blunted cylinders and slabs or sharp-nosed cones and wedges, including example nonequilibrium flow field correlations of numerical solutions available in the literature. Low density nonequilibrium flows with a negligible shock layer atom recombination rate are also examined; as expected, a less restrictive small disturbance similitude law is obtained in this case.

Nomenclature

α	=	atom mass fraction (ρ_A/ρ)
β	=	vibrational relaxation rate parameter, Eq. [8]
d_N	=	nose diameter
D_N	=	nose drag
e_V	=	energy in molecular vibration
γ	=	frozen specific heat ratio
h	=	specific enthalpy of mixture
h_D	=	dissociation energy of molecules (heat of formation of atoms)
k_R	=	recombination rate constant
K_N, K_R, K_V	=	similitude parameters, Eq. [19]
L	=	characteristic length
$\lambda_D, \lambda_V, \lambda_\rho$	=	similitude parameters, Eq. [19]
M_∞	=	freestream Mach number
$\mathfrak{M}_m$	=	molecular weight of undissociated gas
ω	=	recombination rate temperature exponent
p	=	pressure
ρ	=	density
ρ_D	=	characteristic dissociation density
R_M	=	undissociated gas constant
σ	=	shock wave angle
τ	=	characteristic slope
T	=	absolute temperature
T_D	=	characteristic dissociation temperature
T_V	=	characteristic vibration temperature
θ	=	angle of attack
U_∞	=	freestream velocity
u, v	=	Cartesian velocity component perturbations
x, y	=	Cartesian coordinates
$\bar{x}_N, \bar{x}_R$	=	nondimensional similitude coordinates, Eqs. [36] and [38]

Subscripts

A	=	atom
B	=	body surface
eq	=	equilibrium
M	=	molecule
s	=	value immediately behind shock front
∞	=	ambient gas

Received by ARS February 8, 1962; revision received July 24, 1962.

[1] Much of this work was conducted during the author's previous affiliation with the Douglas Aircraft Corporation, Missile and Space Systems Division, Culver City, Calif. Subsequent support was received from the Aerospace Systems Command, U. S. Air Force, under Contract AF04(695)-69.

[2] Member, Technical Staff, Laboratories Division. Member ARS.

The theory of inviscid, hypersonic small disturbance flows (1),[3] including its extension to blunted bodies via the blast wave analogy (2), has proved to be a fruitful analytical tool in aerodynamics and a basis of important similitude laws for the correlation and interpretation of both experimental data and exact numerical solutions. Although this theory does not give an accurate description of the complete flow field on a blunt-nosed body, being invalid near the nose and inaccurate within the high-entropy layer adjacent to the body downstream of the nose, it has nevertheless been very useful in determining asymptotic pressure distributions, shock wave shapes, and the general character of the flow entering the outer portion of the wake on slender bodies. Furthermore, the small disturbance theory has been applied in more advanced theories dealing with entropy layer and boundary layer effects with very fruitful results (3–6).

In view of the significant dissociation and ionization that can occur behind strong shock waves, there is an obvious need to extend the classical small disturbance theory and the resulting similitude laws for a perfect gas to include real gas behavior. Such an extension has been given by Cheng (2) and Sychev (7) for equilibrium dissociation throughout the shock layer on blunted or sharp-nosed slender bodies. However, this theory does not apply to the low ambient densities encountered in high altitude, hypersonic flight above 100,000 to 150,000 ft, where significant departures from equilibrium flow have been demonstrated (8–12). Since many of the important flow field properties are substantially affected under these flight conditions, a further extension of the small disturbance similitude laws to the case of nonequilibrium flow is of practical interest. Furthermore, the possibility of highly nonequilibrium flow in the nozzle of high enthalpy hypersonic testing facilities (which maintains an appreciable dissociation level downstream of the throat) warrants the inclusion of a dissociated freestream condition as well.

Accordingly, this paper presents the hypersonic small disturbance theory and similitude requirements for inviscid, nonequilibrium-dissociated and vibrationally relaxing gas flows over blunt-nosed slender bodies at zero angle of attack. A diatomic gas model is employed, since it describes a family of gases that are of experimental importance and yet is representative of more complex dissociated gas mixtures such as air. The basic relations governing the small disturbance flow in the

[3] Numbers in parentheses indicate References at end of paper.

shock layer, including the integral equation matching the blunt nose and downstream flow regions, are set forth assuming that the gas ahead of, as well as behind, the bow shock envelope may be in an arbitrary state of nonequilibrium dissociation and vibrational excitation. Some related features of the interaction between bluntness and nonequilibrium shock layer dissociation and the importance of freestream dissociation effects will also be discussed. The hypersonic equivalence principle and similitude laws for affinely related, slightly blunted slender bodies are then derived for nonequilibrium flows in diatomic gases or a given gas mixture such as air. These laws are subsequently specialized to blunted cylinders and slabs or sharp-nosed cones and wedges, for which practical nonequilibrium flow field correlations are feasible in certain practical applications. Low density nonequilibrium flows with a negligible shock layer atom recombination rate will also be examined, with a view toward broadening the otherwise rather restrictive small disturbance similitude for bodies such as a blunted cone. Finally, several examples of the nonequilibrium similitude will be presented by correlating the results of some numerical solutions available in the literature.

Governing Relations

Consider the steady, inviscid flow of a reacting gas around a two-dimensional or axially symmetric slender body at zero angle of attack (Fig. 1). The relations governing this flow will be formulated now within the framework of the hypersonic small disturbance theory. Although the discussion is therefore similar in some respects to that in Ref. 2, a more detailed treatment of the thermodynamic and composition variables is required in the present nonequilibrium problem, since the flow is in general neither isentropic nor representable by a single equation of state.

Basic Assumptions

1) The freestream is uniform in velocity, thermodynamic properties, and composition; however, it can be in an arbitrarily dissociated state.

2) The local flow deflection angle θ throughout the shock layer (in radians) is small compared to unity, its magnitude being characterized by an appropriate flow field slope τ.

3) The freestream Mach number M_∞ is large enough compared to unity that the approximation $\sin\sigma \simeq \sigma \sim 0(\tau)$ may be used; however, $M_\infty\tau$ need not be much greater than unity.

4) The velocity perturbations u, v throughout the shock layer are of the same order as their local values at the shock envelope.

5) For blunt-nosed bodies, the characteristic dimensions of the nose are small enough in comparison to the axial dimension of the body that the downstream effects of bluntness may be represented entirely by a concentrated force (drag) at the nose.

6) The flowing medium is a homonuclear diatomic gas in which molecular rotation is completely excited, electronic internal energy states may be neglected, and the molecular vibrational energy states may be represented by simple harmonic oscillator theory.

Assumption 1 is valid for a nonequilibrium dissociated freestream if the change in ambient gas properties over a streamline distance equal to the body length is negligible. Assumptions 2–4 characterize the problem as a hypersonic, small velocity disturbance flow over a slender body and control of the accuracy of the present analysis. However, the corresponding thermodynamic and composition perturbations are not necessarily small; this occurs only when $M_\infty\tau \ll 1$, where the present theory and the classical linearized theory of Prandtl-Glauert for $M_\infty \gg 1$ share a common domain of validity. In cases involving blunt-nosed bodies, assumptions 2 and 3 are clearly not applicable in the vicinity of the nose.

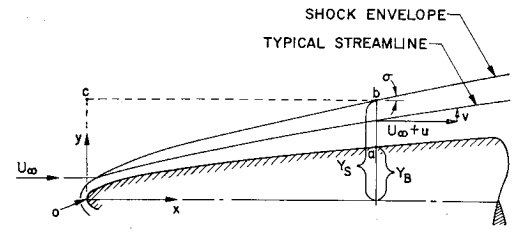

Fig. 1 Flow configuration

Furthermore, assumption 4 is not uniformly valid across the shock layer downstream of the nose, since the magnitude of the streamwise velocity perturbation u within the relatively hot entropy sublayer adjacent to the body is slightly higher than that in the cooler, outer portion of the flow near the shock envelope (5). Assumption 5 implies that the local flow has either originated from an upstream point on the shock envelope at which 2 and 3 are valid or, if originating from the stronger portion of the shock in the vicinity of the nose, has lost all memory of the detailed shock shape and nature of the flow in the nose region. This assumption, as with 4, introduces some inaccuracy in the description of the downstream flow near the body surface (primarily, the density, temperature, and composition distributions), since the entropy sublayer tends to convey downstream the influence of the nose shape as well as the overall energy input of the nose. However, this has a small effect on the pressure and shock shape downstream of the nose when the displacement effect of the entropy sublayer is negligible (4). Moreover, for slender hypersonic bodies with small degrees of blunting, the work in Ref. 5 indicates that the major effects of bluntness on the flow sufficiently far downstream of the nose, including the entropy layer, are accounted for by the foregoing assumptions. For the purpose of examining nonequilibrium flow similitude for slender bodies, it therefore seems reasonable to carry over these assumptions to the present problem.

The diatomic gas model defined in assumption (6) was selected because it affords a clear and yet fairly realistic representation of nonequilibrium gas flows encountered in practice. Indeed, it will be shown that the similitude laws derived on the basis of this model are also directly applicable to complex multicomponent gas mixtures such as air. From another point of view, diatomic gases such as the halogens offer some interesting and advantageous possibilities as a testing environment for simulating certain aspects of hypervelocity flight in air because of their relatively low dissociation energies. Therefore, the possible use of different combinations of diatomic gases, ambient density, and velocity as a means of achieving similitude of nonequilibrium flows over slender bodies will be considered in this paper.

Flow Equations and Boundary Conditions

Following the usual procedure, an order of magnitude analysis of the basic conservation equations is conducted under the foregoing assumptions, dropping terms of order τ^2 or smaller. For a nonequilibrium dissociating diatomic gas, the resulting relations governing the small disturbance flow are

$$U_\infty \frac{\partial \rho}{\partial x} + v \frac{\partial \rho}{\partial y} + \rho\left(\frac{\partial v}{\partial y} + \epsilon \frac{v}{y}\right) \simeq 0$$

$$\begin{cases} \epsilon = 0, \text{ two-dimensional} \\ = 1, \text{ axially symmetric} \end{cases} \qquad [1]$$

$$\rho\left(U_\infty \frac{\partial v}{\partial x} + v \frac{\partial v}{\partial y}\right) + \frac{\partial p}{\partial y} \simeq 0 \qquad [2]$$

$$p = \rho R_M(1 + \alpha)T \qquad [3]$$

$$\rho\left(U_\infty \frac{\partial h}{\partial x} + v \frac{\partial h}{\partial y}\right) \simeq U_\infty \frac{\partial p}{\partial x} + v \frac{\partial p}{\partial y} \qquad [4]$$

$$h = (1 - \alpha)(\tfrac{7}{2}R_M T + e_V) + \alpha(5R_M T + h_D) \quad [5]$$

where e_V is the energy in molecular vibration and h_D is the dissociation energy. Furthermore, the following two rate equations govern the nonequilibrium dissociation and vibrational excitation effects:

$$U_\infty(\partial\alpha/\partial x) + v(\partial\alpha/\partial y) = \mathfrak{R}_{\text{chem}}(\alpha,\rho,T) \quad [6]$$

$$U_\infty(\partial e_V/\partial x) + v(\partial e_V/\partial y) = \mathfrak{R}_{\text{vib}}(\alpha,e_V,\rho,T) \quad [7]$$

where for a diatomic gas (13–15)

$$\mathfrak{R}_{\text{chem}} \simeq \frac{(1+\alpha)k_R T^\omega}{\mathfrak{M}_M{}^2}[(1-\alpha)\rho\rho_D e^{-T_D/T} - \rho^2\alpha^2] \quad [8a]$$

$$\mathfrak{R}_{\text{vib}} \simeq \frac{(1-\alpha)k_V\rho T^\beta}{\mathfrak{M}_M}\exp - \left(\frac{T_V}{T}\right)^{1/3} \times [R_M T_V e^{-T_V/T} - (1 - e^{-T_V/T})e_V] \quad [8b]$$

In Eq. [8], k_R is the recombination rate constant, ω the recombination rate temperature dependence exponent, ρ_D and T_D/R_M are the characteristic dissociation density and temperature (16), k_V and β are vibrational relaxation rate parameters, and T_V is the characteristic vibrational temperature. It may be noted that the local equilibrium solutions to Eqs. [6] and [7] are obtained by setting the bracketed terms on the right sides of Eqs. [8] equal to zero; thus

$$e_{V_{\text{eq}}} = \frac{R_M T_V \exp(-T_V/T)}{1 - \exp(-T_V/T)} \quad [9a]$$

$$\frac{\alpha_{\text{eq}}{}^2}{1 - \alpha_{\text{eq}}} = \frac{\rho_D}{\rho}\exp\left(-\frac{T_D}{T}\right) \quad [9b]$$

Eqs. [1–7], in conjunction with appropriate boundary conditions, are sufficient to determine completely the seven unknowns ρ, p, v, α, T, h, and e_V throughout the entire small disturbance flow field, independently of the longitudinal velocity perturbation u. If desired, u may then be calculated separately from the total enthalpy form of the energy equation as

$$\frac{u}{U_\infty} \simeq -\left(\frac{v}{U_\infty}\right)^2 - \frac{h - h_\infty}{U_\infty{}^2} \quad [10]$$

In general, the flow field so determined is nonisentropic because of the irreversible nature of finite dissociation-recombination and vibrational excitation rate effects. The flow becomes particle isentropic only in the two limiting extremes of chemical behavior: equilibrium flow throughout (Eq. [9]) or chemically and vibrationally frozen flow (right sides of Eqs. [6] and [7] everywhere zero).

Assuming the shock envelope to be a discontinuity, the following relations must be satisfied at the shock envelope:

$$v_s \simeq U_\infty\left(1 - \frac{\rho_\infty}{\rho_s}\right)\frac{dy_s}{dx} \quad [11]$$

$$p_s \simeq p_\infty + \rho_\infty U_\infty{}^2\left(1 - \frac{\rho_\infty}{\rho_s}\right)\left(\frac{dy_s}{dx}\right)^2 \quad [12]$$

$$h_s \simeq h_\infty + U_\infty{}^2\left(1 - \frac{\rho_\infty{}^2}{\rho_s{}^2}\right)\left(\frac{dy_s}{dx}\right)^2 \quad [13]$$

plus Eqs. [3] and [5] evaluated ahead of and behind the shock. Moreover, since the shock thickness is tacitly assumed infinitesimal compared to the vibration and dissociation lengths, one has $\alpha_s = \alpha_\infty$ and $e_{V_s} = e_{V_\infty}$.

At the inner boundary $y = y_B(x)$, one has the condition

$$v_B \simeq U_\infty dy_B/dx \quad [14]$$

Furthermore, in the case of blunt-nosed bodies, the transonic flow in the nose region and the supersonic flow field should be matched along a convenient characteristic that traverses the shock layer slightly downstream of the sonic line. However, as far as the flow far downstream of the nose is concerned, it is sufficient under assumption 5 to represent this matching by an overall mass, momentum, and energy conservation statement for the shock layer. Thus, using the control volume OABC in Fig. 1, the small disturbance flow must satisfy the integral equation

$$D_N + \int_{0^+}^{x} p_B\frac{dy_B}{dx}(2\pi y_B)^\epsilon\,dx \simeq \int_{y_B}^{y_s}\rho\frac{v^2}{2}(2\pi y)^\epsilon\,dy + R_M\int_{y_B}^{y_s}\left\{\left[\frac{5}{2}(1-\alpha)+3\alpha\right]\rho T - \left[\frac{5}{2}(1-\alpha_\infty)+3\alpha_\infty\right]\rho_\infty T_\infty\right\}(2\pi y)^\epsilon\,dy + \int_{y_B}^{y_s}\{[\rho(1-\alpha)e_V - \rho_\infty(1-\alpha_\infty)e_{V\infty}] + h_D[\rho\alpha - \rho_\infty\alpha_\infty]\}(2\pi y)^\epsilon\,dy \quad [15]$$

where the axial extent of the nose region with drag D_N has been neglected (2). Eq. [15] states that the total power input by the nose and afterbody pressure drag appears in the downstream flow as kinetic energy of the transverse motion, an increase in translational and rotational internal energy relative to the freestream, and the energy absorbed in postshock molecular vibration and dissociation. When the afterbody pressure drag integral is small compared to D_N, it is evident that a substantial reduction of the bluntness effect will occur when a large fraction of power is absorbed by dissociation and vibration in the nose region, and subsequent expansion downstream of the nose freezes out a significant percentage of this energy. In this case, the form of Eq. [15] is equivalent to a perfect gas flow with a reduced fictitious nose drag

$$D_N{}^* = D_N - \underbrace{\int_{y_B}^{y_s}\{\rho[(1-\alpha)e_V + \alpha h_D] - \rho_\infty[(1-\alpha_\infty)e_V + \alpha_\infty h_D]\}(2\pi y)^\epsilon dy}_{D_{N\alpha}} \quad [16]$$

where $D_{N\alpha}$ is a constant. In contrast, when the flow remains in equilibrium throughout the shock layer, $D_{N\alpha}$ is not constant but is usually quite small in the supersonic flow region. One may conclude that an appreciable departure from equilibrium in the flow around a slender blunted body can significantly increase the rate of pressure decay along the body downstream of the nose. This effect has been observed and studied in detail by several investigators (9,10).

It should be emphasized that the integral nose matching condition, which neglects the detailed nature of the flow in the nose region, does not yield a completely accurate description of the forementioned nonequilibrium interaction downstream of the nose on blunt bodies. Moreover, most of the shock layer dissociation originates behind the strong portion of the bow shock near the nose, so that the effective drag $D_N{}^*$ depends on the detailed shape (as well as the overall drag) of the nose. Also, the effects of dissociation on the afterbody flow field are mainly communicated downstream by the entropy sublayer, where the small perturbation assumptions are not entirely adequate for describing the detailed flow. Of course, this limitation is somewhat offset by the effectively reduced nose drag at a given distance from the nose. Furthermore, in spite of the comparatively small degree of dissociation which usually prevails outside the entropy sublayer, the presence of nonequilibrium flow and its resulting interplay with the influence of nose bluntness may still have a significant effect on the density, temperature, and pressure distributions outside the entropy layer because of the large dissociation energies involved (11).

In practical applications involving the simulation of hypervelocity flight in advanced wind tunnels, the test gas can be

in a highly nonequilibrium, dissociated state (9,11,17). Therefore, before passing, the possible effects of freestream dissociation on the foregoing flow problem (relative to the flow behavior in an undissociated ambient gas) will be examined briefly in order to gage the significance of α_∞ as a similitude parameter. This may be done by drawing upon the results obtained in some recent theoretical studies of hypersonic flows in dissociated incoming streams (18,19). For a given stream velocity, it was found that the usual spread between frozen and equilibrium states and the initial dissociation rate behind oblique and normal shock waves will decrease significantly when $\alpha_\infty > 0.25$ and can become vanishingly small for sufficiently large values of α_∞. The degree of ambient dissociation required to realize the special case $\alpha_{eqs} = \alpha_\infty$ decreases as the shock strength is decreased. Concerning the effects of freestream dissociation on slender body flow fields, then, one may draw the following conclusions:

1) Small disturbance flows around blunt or sharp-nosed bodies can be much further out of equilibrium (more nearly frozen) than is the case for the same body in an undissociated ambient gas. A greater portion of the flow around a blunted body, for example, would therefore behave as a perfect gas flow with a specific heat ratio pertaining to the freestream.

2) Even in the strong shock region near the nose of a blunted body, where equilibrium usually prevails, the postshock conditions can become nearly frozen when $\alpha_\infty > 0.25$ (19). Hence, the interaction between bluntness and postshock nonequilibrium effects (Eq. [16]) is diminished, since the fraction of power input by the nose which is absorbed in shock layer dissociation and vibration is reduced.

3) The strength and shape of the bow shock assume a decreasing importance in determining the shock layer dissociation level as σ_∞ increases, since the dissociation history of the freestream itself becomes the controlling factor. Consequently, the significance of the entropy layer in communicating downstream the effect of interaction between the effects of bluntness and nonequilibrium dissociation is also diminished. (Further details concerning this point may be found in Ref. 19.)

In view of these conclusions, it is clear that freestream dissociation can have an important influence on the flow field around a blunt or sharp-nosed body and therefore will be a significant parameter for models tested in highly nonequilibrium gas streams.

The Equivalence Principle

The equivalence of a steady hypersonic flow past a slender three-dimensional body to the corresponding unsteady flow produced in the cross plane was originally demonstrated by Hayes (20) and later extended to equilibrium reacting gas flows over blunt-nosed bodies by Cheng (2). Although perhaps not generally recognized, this equivalence principle is applicable to nonequilibrium flow problems as well. For it may be seen easily that, under the transformation $x = U_\infty t$, Eqs. [1–14] pass over to a set of relations that govern the corresponding motion of the same gas in the body cross-plane as seen by an observer at rest with respect to the undisturbed gas. As shown by Cheng (2), the effect of nose bluntness in the steady problem (to the degree of approximation represented by Eq. [15]) is then equivalent to an unsteady blast wave in one less space dimension, Eq. [15] playing the role of an initial condition relating the initial blast energy to the nose drag of the body. Here, of course, some of the initial blast energy may be absorbed in unsteady nonequilibrium vibrational excitation and dissociation. It may be seen that the foregoing proof rests entirely on the approximations $U \approx U_\infty$ and $\sin\sigma \simeq \sigma$ and does not involve specifying the detailed form of the equations of state or the vibrational and chemical rates. Therefore, within the framework of the small disturbance assumptions, the equivalence principle is, in fact, generally applicable to any nonequilibrium reacting multicomponent gas mixture.

Nonequilibrium Flow Similitude

The nonlinear set of Eqs. [1–14] constitutes the formal mathematical problem for small disturbance diatomic gas flows. These relations provide a basis for possible extension of the analytical solutions that have been obtained for a perfect gas (1, 4–6, 21) to the case of nonequilibrium dissociated flows. However, the author will not deal with this problem here but will proceed to an examination of the various similitude laws pertaining to nonequilibrium flows around affinely related slender bodies.

General Similitude for Affinely Related Bodies

Now consider a family of steady nonequilibrium small disturbance flows related under the following transformation of variables:

$$\bar{x} = \frac{x}{L} \qquad \bar{y} = \frac{y}{\tau L} \qquad \bar{u} = \frac{u}{\tau^2 U_\infty}$$

$$\bar{v} = \frac{v}{\tau U_\infty} \qquad \bar{\rho} = \frac{\rho}{\rho_\infty} \qquad \bar{p} = \frac{p}{p_\infty} \qquad [17]$$

$$\bar{T} = \frac{T}{T_\infty} \qquad \bar{h} = \frac{h - h_\infty}{R_M T_\infty (1 + \alpha_\infty)} \qquad \bar{e_V} = \frac{e_V}{R_M T_\infty}$$

where L is an arbitrary reference length. Then introducing the frozen freestream Mach number

$$M_\infty = \frac{U_\infty}{[\bar{\gamma}_\infty R_M T_\infty (1 + \alpha_\infty)]^{1/2}} \qquad [18]$$

where $\bar{\gamma}_\infty = [7(1 - \alpha_\infty) + 10\,\alpha_\infty]/[5(1 - \alpha_\infty) + 6\alpha_\infty]$ is the frozen specific heat ratio of the freestream, and the parameters

$$\lambda_D = T_D/T_\infty \qquad \lambda_V = T_V/T_\infty \qquad \lambda\rho = \rho_D/\rho_\infty$$

$$K_N = M_\infty^{(3+\epsilon)/(1+\epsilon)}\, C_{D_N}^{1/(1+\epsilon)}\, \frac{d_N}{L}$$

$$\left.\begin{aligned} d_N &= \text{nose diameter} \\ C_{D_N} &= \frac{2D_N}{\rho_\infty U_\infty^2 (d_N/2)(\pi d_N/2)^\epsilon} \end{aligned}\right\} \qquad [19]$$

$$K_R = \frac{\text{residence time}}{\text{reaction time}} = \frac{k_R L T_\infty^{\omega} \rho_\infty^2}{U_\infty \mathfrak{M}_M^2}$$

$$K_V = \frac{\text{residence time}}{\text{vibrational relaxation time}} = \frac{k_V L T_\infty^{\beta} \rho_\infty}{U_\infty \mathfrak{M}_M}$$

Eqs. [1–15] may be written as follows:

$$\frac{\partial \bar{\rho}}{d\bar{x}} + \bar{v}\frac{\partial \bar{\rho}}{\partial \bar{y}} + \bar{\rho}\left(\frac{\partial \bar{v}}{\partial \bar{y}} + \epsilon\frac{\bar{v}}{\bar{y}}\right) \simeq 0 \qquad [20]$$

$$\bar{\rho}\left(\frac{\partial \bar{v}}{\partial \bar{x}} + \bar{v}\frac{\partial \bar{v}}{\partial \bar{y}}\right) + \frac{\partial \bar{p}/\partial \bar{y}}{\bar{\gamma}_\infty (M_\infty \tau)^2} \simeq 0 \qquad [21]$$

$$\bar{p} = \bar{\rho}\bar{T}\left(\frac{1 + \alpha}{1 + \alpha_\infty}\right) \qquad [22]$$

$$\bar{\rho}\left(\frac{\partial \bar{h}}{\partial \bar{x}} + \bar{v}\frac{\partial \bar{h}}{\partial \bar{y}}\right) \simeq \frac{\partial \bar{p}}{\partial \bar{x}} + \bar{v}\frac{\partial \bar{p}}{\partial \bar{y}} \qquad [23]$$

$$\bar{h} = \left(\frac{\alpha - \alpha_\infty}{1 + \alpha_\infty}\right)\lambda_D + \frac{(1 - \alpha)\bar{e_V} - (1 - \alpha_\infty)\bar{e_V}_\infty}{1 + \alpha_\infty} + \left(\frac{\bar{\gamma}_\infty}{\bar{\gamma}_\infty - 1}\right)\left\{\left[\frac{7(1 + \alpha) + 10\alpha}{7(1 - \alpha_\infty) + 10\alpha_\infty}\right]\bar{T} - 1\right\} \qquad [24]$$

$$\frac{\partial \alpha}{\partial \bar{x}} + \bar{v}\frac{\partial \alpha}{\partial \bar{y}} \simeq K_R(1+\alpha)(\bar{T})^{\omega} \times \left[(1-\alpha)\lambda_\rho\,\bar{\rho}\exp\left(-\frac{\lambda_D}{\bar{T}}\right) - \bar{\rho}^2\alpha^2\right] \quad [25]$$

$$\frac{\partial \overline{e_V}}{\partial \bar{x}} + \bar{v}\frac{\partial \overline{e_V}}{\partial \bar{y}} \simeq K_V(1-\alpha)(\bar{T})^{\beta}\exp-\left(\frac{\lambda_V}{\bar{T}}\right)^{1/3} \times [e^{-\lambda_V/\bar{T}} - (1-e^{-\lambda_V/\bar{T}})\overline{e_V}] \quad [26]$$

and

$$u \simeq -\bar{v}^2 + [\bar{h}/\bar{\gamma}_\infty(M_\infty\tau)^2] \quad [27]$$

The shock boundary conditions at $\bar{y} = \bar{y}_s(\bar{x})$ become

$$\bar{v}_s \simeq \left(\frac{\bar{\rho}_s - 1}{\bar{\rho}_s}\right)\frac{d\bar{y}_s}{d\bar{x}} \quad [28]$$

$$\bar{p}_s \simeq 1 + \bar{\gamma}_\infty(M_\infty\tau)^2\left(\frac{\bar{\rho}_s-1}{\bar{\rho}_s}\right)\left(\frac{d\bar{y}_s}{d\bar{x}}\right)^2 \quad [29]$$

$$\bar{h}_s \simeq \bar{\gamma}_\infty(M_\infty\tau)^2\left(\frac{\bar{\rho}_s{}^2-1}{\bar{\rho}_s{}^2}\right)\left(\frac{d\bar{y}_s}{d\bar{x}}\right)^2 \quad [30]$$

plus [22] and [24] evaluated at the shock and $\alpha_s = \alpha_\infty$, $\overline{e_{V_s}} = \overline{e_{V\infty}}$. At the inner boundary, one has

$$\bar{v}_B \simeq d\bar{y}/d\bar{x} \quad [31]$$

Finally, the blunt-nose matching condition transforms to

$$\frac{\bar{\gamma}_\infty\pi^\epsilon}{(2)^{2+\epsilon}}\left(\frac{K_N}{M_\infty\tau}\right)^{1+\epsilon} + \int_{0^+}^{\bar{x}} p_B\frac{d\bar{y}_B}{d\bar{x}}(2\pi\bar{y}_B)^\epsilon d\bar{x} \simeq \frac{\bar{\gamma}_\infty(M_\infty\tau)^2}{2}\int_{\bar{y}_B}^{\bar{y}_s}\bar{\rho}\bar{v}^2(2\pi\bar{y})^\epsilon d\bar{y} + \left(\frac{1}{\bar{\gamma}_\infty - 1}\right) \times \int_{\bar{y}_B}^{\bar{y}_s}\left\{\left[\frac{5(1-\alpha)+6\alpha}{5(1-\alpha_\infty)+6\alpha_\infty}\right]\bar{\rho}\bar{T} - 1\right\}(2\pi y)^\epsilon d\bar{y} + \frac{1}{1+\alpha_\infty}\int_{\bar{y}_B}^{\bar{y}_s}[\bar{\rho}(1-\alpha)\overline{e_V} - (1-\alpha_\infty)\overline{e_{V\infty}}](2\pi\bar{y})^\epsilon d\bar{y} + \frac{\lambda_D}{1+\alpha_\infty}\int_{\bar{y}_B}^{\bar{y}_s}(\bar{\rho}\alpha - \alpha_\infty)(2\pi\bar{y})^\epsilon d\bar{y} \quad [32]$$

The solution to the foregoing equations is seen to be the same for all slender bodies of the form $y_B/\tau L = f(x/L)$ when each of the following parameters is held constant: α_∞, λ_D, λ_V, λ_ρ, $\overline{e_{V\infty}}$; ω, β; K_R, K_V, K_N, and $M_\infty\tau$. Furthermore, this similitude property shows that the nonequilibrium small disturbance flow fields around these affinely related bodies are correlated in the following way:

$$\left.\begin{array}{l} p/p_\infty \\ \rho/\rho_\infty \\ T/T_\infty \\ \alpha \\ (h-h_\infty)/R_MT_\infty(1+\alpha_\infty) \\ v/U_\infty\tau,\ u/U_\infty\tau^2 \end{array}\right\} = \underbrace{f(\alpha_\infty, \overline{e_{V\infty}}, \lambda_D, \lambda_V, \lambda_\rho;}_{\text{(I) incoming gas properties}} \underbrace{\omega, \beta, K_R, K_V;}_{\text{(II) nonequilibrium flow parameters}} M_\infty\tau, K_N;\ \epsilon, x/L, y/\tau L) \quad [33]$$

with a shock surface

$$y_s/\tau L = f(\alpha_\infty, \overline{e_{V\infty}}, \lambda_D, \lambda_V, \lambda_\rho;\ \omega, \beta, K_R, K_V;\ M_\infty\tau, K_N;\ \epsilon, x/L) \quad [34]$$

These relations generalize the similitude laws given by Cheng to the case of a family of nonequilibrium dissociated and vibrationally excited diatomic gas flows over blunt-nosed slender bodies in a nonequilibrium dissociated freestream. Here, the appropriate real gas similitude parameters have been divided into two basic groups: (I) the chemical and vibration properties of the incoming stream (α_∞, $\overline{e_{V\infty}}$) and three parameters (λ_ρ, λ_D, λ_V) involving the ambient state and physical properties of the gas; and (II) the additional similitude parameters required in the presence of a nonequilibrium small disturbance flow, namely the reaction rate temperature exponents ω and β and the characteristic (flow time/relaxation time) ratios for a dissociation-recombination and vibrational excitation (K_R, K_V). It should be noted that α_∞ and $\overline{e_{V\infty}}$ are independent parameters determined by the particular nonequilibrium flow history ahead of the body unless the freestream is in equilibrium, in which case they become functions of λ_D, λ_ρ, and λ_V. Therefore, according to the previous discussion, testing in dissociated gas streams typical of advanced hypersonic wind tunnels cannot be expected to duplicate free flight flow conditions under the foregoing similitude unless the test stream is in equilibrium or is less than approximately 10% nonequilibrium dissociated.[4]

With the exception of α_∞, $\overline{e_{V\infty}}$, and the reaction rate temperature exponents ω and β, it is observed from Eq. [33] that the physical properties of the gas and the ambient state variables ρ_∞, T_∞ do not enter the similitude separately but in various nondimensional combinations with each other. Consequently, the foregoing similitude can conceivably be achieved in two different ways: 1) by employing different combinations of ρ_∞ and T_∞, U_∞, and body scale in conjunction with various types of diatomic gases;[5] or 2) by using a fixed type of gas together with a fixed ambient gas state ρ_∞, T_∞. The former approach has the disadvantage of being incapable of simulating both vibration and dissociation effects simultaneously, since the ratios T_V/T_D and K_V/K_R differ considerably from one diatomic gas to another. Hence, one would be confined to vibrationally excited flows with negligible dissociation or to flows in which the vibrational energy is either negligible in comparison to the energy in dissociation or completely excited ($\overline{e_V} = \overline{e_{V\text{eq}}} = \bar{T}$). Nevertheless, even in this restricted sense, the use of different diatomic gases may be useful for simulating certain gross aerothermodynamic features of hypervelocity flight in ballistic ranges. The second method, in which each of the physical properties T_D, T_V, ρ_D, ω, and β is fixed, results in the following simplified similitude law:

$$\left.\begin{array}{l} p/p_\infty \\ \rho/p_\infty \\ T/T_\infty \\ \alpha \\ (h-h_\infty)/R_MT_\infty(1+\alpha_\infty) \\ v/U_\infty\tau,\ u/U_\infty\tau^2 \end{array}\right\} = f[\alpha_\infty, \overline{e_{V\infty}}, \rho_\infty, T_\infty; k_R'(L/U_\infty); M_\infty\tau, K_N;\ \epsilon, x/L, y/\tau L] \quad [35]$$

where $k_R' = k_RT_\infty{}^\omega\rho_\infty{}^2/\mathfrak{M}_M{}^2$ is a constant. With the exception of the additional parameter L/U_∞, the similitude defined by this Eq. [35] is the same as that obtained by Cheng for equilibrium flows. Eq. [35] is, of course, implied directly by the generalized equivalence principle for small disturbance, nonequilibrium gas flows. Therefore, it is clear that, if α_∞ and $\overline{e_{V\infty}}$ are understood to represent *each* of the components in a multicomponent gas, the similitude [25] applies to an arbitrary reacting gas mixture such as air, as well as to a given diatomic gas. Furthermore, since the type of gas is fixed, this similitude law governs the energy in electronic excitation, ionization, and gaseous radiation, as well as the effects of dissociation and vibration. It may be noted that only two arbitrary geometrical scaling factors (τ and L) appear in the three basic similitude parameters $M_\infty\tau$, K_N, and K_R or K_V; hence, under the required scaling of the ambient state-gas property conditions, the simulation of nonequilibrium flows

[4] In such applications, the value of $\overline{e_{V\infty}}$ may usually be neglected.

[5] The parameters ω and β must also be fixed; however, existing theoretical and experimental evidence indicates that ω and β are indeed approximately the same for a variety of diatomic gases (13–15).

over blunt-nosed slender bodies by either of these two methods abolishes any freedom in choosing the scale of the working models. However, if the shock layer recombination rate can be neglected in comparison to the dissociation rate, a less restrictive nonequilibrium similitude is obtained, as will be subsequently shown.

In the limiting case of equilibrium flow throughout the shock layer (K_R, $K_V \to \infty$), the parameters in Group II of Eq. [33] drop out, and one obtains a generalized equilibrium similitude law for a family of diatomic gases under which the ambient density and temperature need not be simulated. Eq. [35], of course, reduces to precisely Cheng's result (2) for an arbitrary gas mixture in equilibrium. In the opposite extreme of completely frozen flow ($\alpha = \alpha_s = \alpha_\infty$, $\overline{e_V} = \overline{e_{V_s}} = \overline{e_{V\infty}}$, $K_R = K_V \to 0$), Eqs. [20–32] show that all of the similitude parameters in Groups I and II can be replaced by the single parameter $\tilde{\gamma}_\infty$,[6] and Eq. [33] reduces to the similitude law for a perfect gas. Of course, all of the similitude requirements in Eq. [33] or [35] must be met when any portion of the shock layer flow departs from equilibrium, regardless of the assumed state of the gas at the shock. A special exception is the case of an analytical flow model involving a frozen shock layer and an equilibrium shock envelope (9,10) which is governed by the *equilibrium* flow similitude. However, it should be emphasized that the flow field defined by this simplified model does not in general behave as a perfect gas with specific heat ratio $\tilde{\gamma}_\infty$; this limiting situation is realized only in the presence of a highly nonequilibrium dissociated freestream when $\alpha_{s_{eq}} = \alpha_\infty$.

Special Similitude for Cylinders and Cones

For a blunted wedge or cone, the afterbody is defined by $y_B = \tau x$ (τ being the cone or wedge half-angle), whereas L becomes an arbitrary scaling factor, since it cannot be used to generate any new members in a family of affinely related bodies. In the two limiting extremes of equilibrium or frozen flow, L may be chosen appropriately to obtain a similitude law covering the combined effects of nose bluntness and afterbody disturbances (2). As previously pointed out, departures from nonequilibrium pose further requirements on this similitude which eliminate a free choice of body scale. However, if $M_\infty\tau$ or K_N drop out of the problem, a nonequilibrium flow similitude is obtained which is comparable to the similitude for blunted cones in an equilibrium or frozen flow. Therefore, the special cases of either blunted cylinders and slabs or sharp-nosed cones and wedges will be examined.

Consider first blunt-nosed, slender cylindrical bodies at zero angle of attack. To prevent ambiguity in interpreting τ when $dy_B/dx = 0$, let $\tau = M_\infty^{-1}$. Following Cheng, take $L = M_\infty^{(3+\epsilon)/(1+\epsilon)} C_{DN}^{1/(1+\epsilon)} d_N (K_N = 1)$, thereby obtaining the following nonequilibrium similitude from [33]:

$$\left.\begin{array}{l} p/p_\infty \\ \rho/\rho_\infty \\ T/T_\infty \\ \alpha \\ \dfrac{h - h_\infty}{R_M T_\infty (1 + \alpha_\infty)} \\ v/U_\infty\tau,\ u/U_\infty\tau^2 \end{array}\right\} = f[\alpha_\infty, \overline{e_V}, \lambda_D, \lambda_V, \lambda_\rho;\ K_V/K_R, K_{RN};\ \epsilon, M_\infty(y/x), \underbrace{M_\infty^{(3+\epsilon)/(1+\epsilon)} C_{DN}^{1/(1+\epsilon)} (d_N/x)}_{1/\bar{x}_N}] \quad [36]$$

and

$$M_\infty(y_s/x) = f(\alpha_\infty, \overline{e_V}_\infty, \lambda_D, \lambda_V, \lambda_\rho;\ \omega, \beta, K_V/K_R, K_R;\ \epsilon, \bar{x}_N) \quad [37]$$

where $K_{RN} = (k_R T_\infty^{\omega} \rho_\infty^2 / \mathfrak{M}_M^2 U_\infty) M_\infty^{(3+\epsilon)/(1+\epsilon)} C_{DN}^{1/(1+\epsilon)} d_N$ may be viewed as the ratio of the lengths characterizing the effects of nonequilibrium reaction and nose bluntness on the small disturbance flow. When $(y_B/x)M_\infty \approx M_\infty(d_N/x) \ll 1$, one sees that the pressure distributions and shock shapes on all blunt-nosed cylinders or slabs with the same K_{RN} will be correlated by the nondimensional distance $\bar{x}_N$ when the ambient state-gas property conditions are properly scaled. Obviously, these correlations become independent of the parameter K_{RN} in the limits of completely equilibrium ($K_{RN} \to \infty$) or completely frozen flow ($K_{RN} \to 0$).

Turning to the case of sharp-nosed cones and wedges ($K_N = 0$), an appropriate nonequilibrium similitude may be obtained by choosing $L = \mathfrak{M}_M^2 U_\infty / k_R T_\infty^{\omega} \rho_\infty^2$ such that $K_R = 1$ (or, in the case of vibrational relaxation only, $L = \mathfrak{M}_M U_\infty^2 / k_V T_\infty^{\beta} \rho_\infty$). One then arrives at the following rule from Eqs. [33] and [34]:

$$\left.\begin{array}{l} p/p_\infty \\ \rho/\rho_\infty \\ T/T_\infty \\ \alpha \\ (h - h_\infty)/R_M T_\infty (1 + \alpha_\infty) \\ v/U_\infty\tau,\ u/U_\infty\tau^2 \end{array}\right\} = f(\alpha_\infty, \overline{e_V}_\infty, \lambda_D, \lambda_V, \lambda_\rho;\ \omega, \beta, K_V/K_{RN};\ M_\infty\tau;\ \epsilon, M_\infty y/x, \underbrace{k_R \rho_\infty^2 T_\infty^{\omega} x / \mathfrak{M}_M^2 U_\infty}_{\bar{x}_R}) \quad [38]$$

$$M_\infty(y_s/x) = f(\alpha_\infty, \overline{e_V}_\infty, \lambda_D, \lambda_V, \lambda_\rho; \omega, \beta, K_V/K_R; M_\infty\tau, \overline{x_R}) \quad [39]$$

These relations predict that the nonequilibrium pressure distributions and shock shapes on a family of affinely related slender cones or wedges are functions only of the nondimensional "reaction coordinate" $\overline{x_R}$ (the ratio of the local distance to a characteristic relaxation length) when $M_\infty\tau$ = constant. Clearly, these distributions become independent of $\overline{x_R}$ near the tip ($\overline{x_R} \to 0$, frozen flow) and far downstream at sufficiently large $\overline{x_R}$ (equilibrium flow).

It may be observed that only one arbitrary scaling parameter occurs in the foregoing special similitude laws (i.e., the nose radius in the variables K_{RN}, $\overline{x_N}$ for blunted slabs and cylinders, and the body slope τ in $M_\infty\tau$, $\overline{x_R}$ for sharp cones and wedges). Consequently, Eqs. [36–39] are of rather limited practical interest as a means of correlating experimental data or numerical solutions obtained under various arbitrary conditions. On the other hand, in a planned experiment or analysis, the foregoing similitude laws provide a practical basis for simulating the same nonequilibrium effects between two or more affinely related bodies such that all the local pressure distributions, shock shape, etc., are correlated by the same nondimensional streamwise coordinate.

Negligible Recombination

Gibson (22) and Hall, Eschenroeder, and Marrone (11) have recently shown that a very useful hypersonic similitude governs the nonequilibrium dissociated flow in the stagnation region of geometrically similar blunt bodies when the ambient density is sufficiently low that the shock layer atom recombination rate ($\sim\rho_\infty^2$) may be neglected in comparison to the corresponding dissociation rate ($\sim\rho_\infty$). Now, under these flight conditions, the assumption of negligible recombination also would be applicable to the small disturbance flow fields on both blunt and sharp-nosed slender bodies. Therefore, it is of interest to examine the consequences of introducing this assumption into foregoing nonequilibrium similitude laws.

When the recombination term $\rho^2\alpha^2$ in Eq. [25] is neglected, the general similitude ([33] and [34]) reduces to

$$\left.\begin{array}{l} p/p_\infty \\ \rho/\rho_\infty \\ T/T_\infty \\ \alpha \\ (h - h_\infty)/R_M T_\infty (1 + \alpha_\infty) \\ v/U_\infty\tau,\ u/U_\infty\tau^2 \end{array}\right\} = f(\alpha_\infty, \overline{e_V}_\infty, \lambda_D, \lambda_V;\ \omega, \beta, K_V/K_R, K_R^*;\ M_\infty\tau, K_N;\ \epsilon, x/L, y/\tau L) \quad [40]$$

$$M_\infty y_s/x = f(\alpha_\infty, \overline{e_V}_\infty, \lambda_D, \lambda_V; \omega, \beta, K_V/K_R, K_R^*;\ M_\infty\tau, K_N;\ \epsilon, x/L) \quad [41]$$

where

$$K_R^* = \lambda\rho K_R = \rho_D k_R T_\infty^{\omega} \rho_\infty L / \mathfrak{M}_M^2 U_\infty \quad [42]$$

[6] By continuity, the last two terms in Eq. [32] vanish when $\alpha = \alpha_\infty$ and $\overline{e_V} = \overline{e_V}_\infty$.

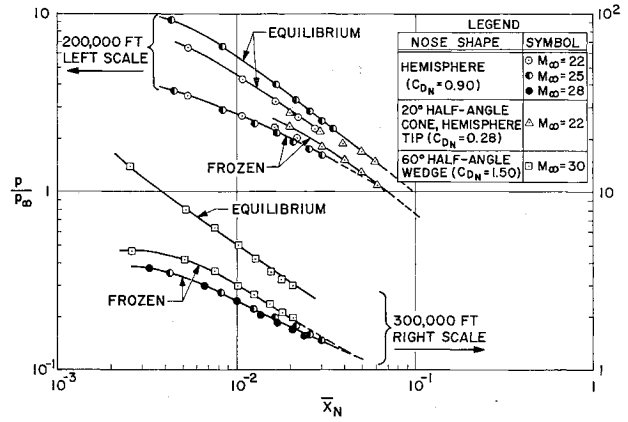

Fig. 2 Correlation of afterbody pressure distributions on blunt-nosed cylinders in air (theory of Ref. 10)

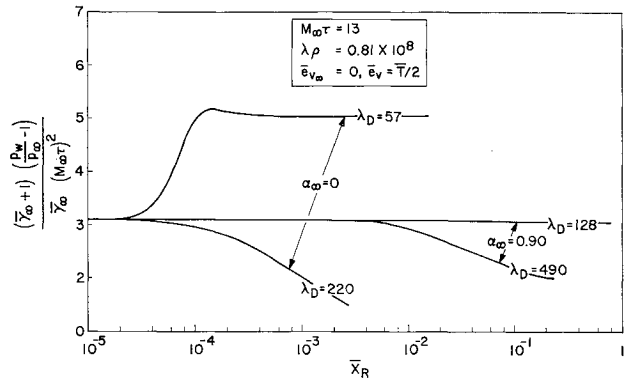

Fig. 3a Nonequilibrium diatomic gas flow over a sharp wedge: surface pressure correlation (theory of Ref. 12)

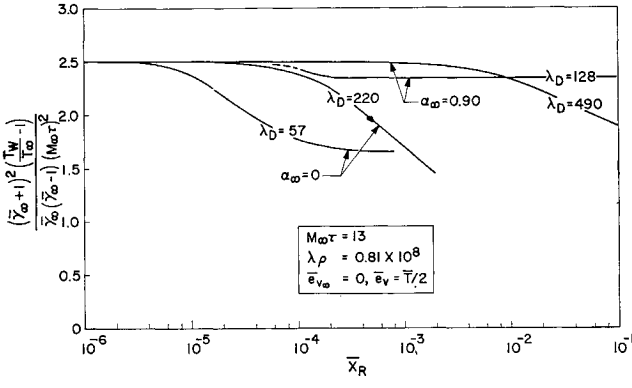

Fig. 3b Nonequilibrium diatomic gas flow over a sharp wedge: surface temperature correlation (theory of Ref. 12)

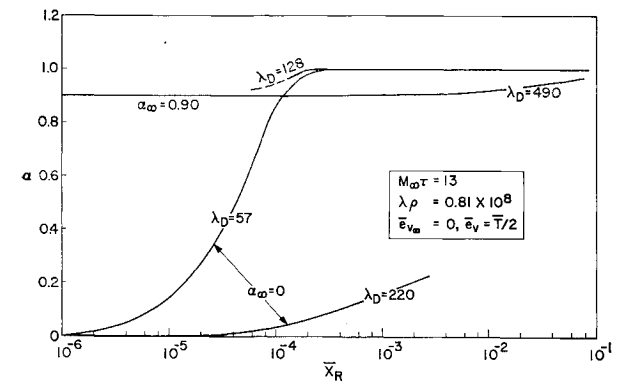

Fig. 3c Nonequilibrium diatomic gas flow over a sharp wedge: surface atom concentration (theory of Ref. 12)

It is seen that $\lambda\rho$ has been absorbed into a new characteristic (flow time/relaxation time) parameter K_R*.[7] Consequently, the nonequilibrium small disturbance flow similitude for bodies such as a blunted cone is considerably broadened, since three independent scaling variables (ρ_∞, L, τ) are available to fix the basic similitude parameters $M_\infty\tau$, K_N, and K_R*. Eq. [40] is applicable either to a family of diatomic gases (with T_D/T_∞ = const, ω, β = const) or to a fixed, arbitrary gas mixture (with T_∞ = const) when α_∞, $\bar{e}_{V_\infty}$ are understood as referring to each component. In the latter application, for example, the similitude for blunted slabs or cylinders simplifies to

$$\left.\begin{array}{l} p/p_\infty \\ \rho/\rho_\infty \\ T/T_\infty \\ \alpha \\ (h-h_\infty)/R_M T_\infty(1+\alpha_\infty) \\ v/U_\infty\tau,\ u/U\tau^2 \end{array}\right\} = f[\alpha_\infty, \bar{e}_{V_\infty}, T_\infty, \text{const} \times \rho_\infty d_N (M_\infty{}^2 C_{D_N})^{1/(1+\epsilon)}; M_\infty(y/x), \bar{x}_N] \quad [43]$$

Similarly, for sharp-nosed cones and wedges in a fixed gas, one has

$$\left.\begin{array}{l} p/p_\infty \\ \rho/\rho_\infty \\ \cdot \\ \cdot \\ \cdot \\ \text{etc.} \end{array}\right\} = f[\alpha_\infty, \bar{e}_{V_\infty}, T_\infty;\ M_\infty\tau;\ M_\infty(y/x), \text{const} \times (\rho_\infty x/M_\infty)] \quad [44]$$

According to Eq. [44], one may scale the local nonequilibrium flow around all affinely related slender cones or wedges at different ambient densities or Mach numbers by keeping $\rho_\infty x/M_\infty$ constant.

For nonequilibrium, low density flows around blunt-nosed slender bodies where the atom recombination rate is negligible everywhere in the shock layer, the question arises as to the compatibility between the foregoing small disturbance similitude and the similitude law proposed by Gibson for the flow in the vicinity of the nose on the same body. Now, according to the latter law, the appropriately nondimensionized stagnation region flow is a universal function of the parameters α_∞, $\bar{e}_{V_\infty}$, ω, β, $\lambda_D/M_\infty{}^2$, and K_{RN}* = $(\rho_D/\rho_\infty)K_{RN}$ for all *geometrically similar* nose shapes (C_{D_N} = const). Therefore, a comparison with Eq. [33] shows that the corresponding small disturbance flow downstream of the nose is also scaled if M_∞ and the afterbody slope τ are fixed. That is, Gibson's similitude applies to the entire flow field when the afterbody shapes are also geometrically similar. However, it does not scale the downstream flow around affinely related afterbodies ($M_\infty\tau$ = const) except in those regions where the gas is completely frozen in dissociation from the shock envelope.

Some Examples of Nonequilibrium Field Correlations

Although nonequilibrium flows in the stagnation region of blunted bodies have been studied in great detail theoretically, there are comparatively few solutions that lie within the scope of the hypersonic small disturbance theory. Furthermore, there is at the present time nothing in the way of experimental work concerning such flows. Therefore, only two rather limited examples of the foregoing nonequilibrium similitude laws can be given here, based upon the numerical results available in Refs. 10 and 12.

Blunted Cylinders

A detailed analysis of hypersonic, reacting air flow around blunted cylinders with various nose shapes, altitude, M_∞, and a perfect ambient gas has been given by Vaglio-Laurin and

[7] This is also reflected in the special similitude laws [36-39], $k_R\rho_\infty{}^2$ being replaced by $k_{RD}\rho_D\rho_\infty$.

Bloom (10), assuming either equilibrium flow or a chemically frozen shock layer with an equilibrium shock envelope. A correlation of the resulting afterbody pressure distributions according to Eq. [36] is presented in Fig. 2. Since these solutions were restricted to regions rather close to the nose ($x/d_N \leq 20$), the agreement with the predictions of the small disturbance similitude is understandably poor for most of the data shown in this Fig. 2. Nevertheless, one can perceive a tendency for p_B/p_∞ to become a universal function of the similitude coordinate $\overline{x_N}$ in both the equilibrium and frozen flow models (at a given altitude) for sufficiently large $\overline{x_N}(x/d_N > 20)$. Furthermore, Fig. 2 illustrates reasonably well that the interaction between nonequilibrium dissociation and bluntness effects can substantially lower the local pressure at a given distance downstream of the nose.

Nonequilibrium Flow Over a Sharp Wedge

Capieux and Washington (12) have recently presented a theoretical analysis of nonequilibrium dissociated, vibrationally frozen diatomic gas flows over a sharp-nosed wedge at hypersonic speeds, including a dissociated freestream. Their numerical results pertain to a fairly slender wedge ($\tau \simeq 0.4$) and therefore should be governed by the nonequilibrium similitude law [38]. The attendant correlation of the pressure, temperature, and atom mass fraction distributions on the wedge surface for $\lambda\rho$ and $M_\infty\tau$ constant is presented in Figs. 3a, 3b, and 3c, respectively. The essential features of the nonequilibrium similitude for diatomic gas flows are clearly illustrated by these figures. Thus, for sufficiently small $\overline{x_R}$ (frozen flow at the tip), the gas properties are seen to be independent of both $\overline{x_R}$ and λ_D with p_B/p_∞ and T_B/T_∞ a function of $M_\infty\tau$ and γ_∞ only. With increasing $\overline{x_R}$, the flow relaxes toward equilibrium and exhibits a growing dependence on the parameters λ_D and α_∞. At sufficiently large $\overline{x_R}$, the flow reaches equilibrium and ceases to be a function of $\overline{x_R}$; however, both λ_D and α_∞ remain as significant similitude parameters.

In connection with these theoretical results, one may observe that the nonequilibrium effects on the pressure and temperature distributions are quite significant even when the corresponding degrees of dissociation are not large. As previously mentioned, this is to be expected because of the large dissociation energies involved. A similar conclusion may be drawn from the correlation of equilibrium dissociated air properties for slender wedges presented in Ref. 2. Capieux and Washington's work also serves to justify the present emphasis concerning the importance of the freestream dissociation α_∞ in the similitude of small disturbance flows. In particular, Fig. 3 shows clearly that the propensity of the post-shock flow to remain frozen increases significantly with the atom concentration ahead of the shock.

Concluding Remarks

Aside from the inherent limitations of the hypersonic small disturbance theory, the practical applications of the foregoing similitude laws are restricted in two major respects. First, no consideration has been given to flows involving angle for attack effects. However, it may be seen by writing $y_B/\tau L = f(x/L, \theta/\tau)$ that the nonequilibrium similitude can be extended to small angles of attack θ by adding θ/τ to the similitude. Moreover, for very slender blunted bodies at large angles of attack, an extension of the present analysis can be made following the general approaches of Cheng and Sychev. Second, and perhaps most important, the effects of viscosity have been omitted from the analysis. Consequently, the present results are applicable to the inviscid flow outside the boundary layer only in those body regions and for those flight regimes wherein the boundary layer-induced pressure field may be neglected. For sufficiently low local Reynolds numbers, the viscous interaction effects will modify the present inviscid equilibrium flow similitude by further introducing the interaction parameter $\bar{\chi}$, the ratio of the wall temperature to T_∞, the viscosity temperature-dependence exponent, and the Prandtl and Lewis numbers of the gas. If the latter three properties have a significant influence on the boundary layer-induced pressure, the possibility of using different diatomic gases discussed previously may be compromised unless these properties are very nearly the same for all the gases considered. Moreover, since the boundary layer displacement effect depends on the streamwise rate of change of the integrated mass flow deficiency across the boundary layer (which in turn is sensitive to the temperature and composition profiles), the nonequilibrium history of the flow within and external to the boundary layer may be significant in determining the viscous interaction effect in dissociated flows. For the same reason, the surface recombination rate (catalytic efficiency) along the body also may enter the problem; this has been observed in some theoretical calculations of boundary layer-induced interactions with frozen dissociated flows reported in Ref. 9. Accordingly, an additional similitude parameter characterizing the Dahmkohler number (diffusion time/surface reaction time) for atom recombination of the body surface would occur in the inviscid similitude when viscous interaction effects in nonequilibrium dissociated gas flows are important.

Acknowledgment

The author would like to express his sincere appreciation to S. H. Lam for his stimulating comments and criticisms concerning the manuscript.

References

1 Hayes, W. D. and Probstein, R. F., *Hypersonic Flow Theory* (Academic Press, New York, 1959), p. 30.

2 Cheng, H. K., "Similitude of hypersonic real gas flows over slender bodies with blunted noses," J. Aero/Space Sci. **26,** 575–585 (1959).

3 Hayes, W. D. and Probstein, R. F., "Viscous hypersonic similitude," J. Aero/Space Sci. **26,** 815–824 (1959).

4 Cheng, H. K., Hall, G. J., Golian, T. C., and Hertzberg, A., "Boundary layer displacement and leading edge bluntness effects in high temperature hypersonic flow," J. Aero/Space Sci. **28,** 353–381 (1961).

5 Yakura, J. K., "A theory of entropy layers and nose bluntness in hypersonic flow," ARS Preprint 1983-61 (August 1961).

6 Chernyi, G. G., "Effect of slight blunting of leading edge of an immersed body on the flow around it at hypersonic speeds," NASA Tech. Transl. F-35 (1960).

7 Sychev, V. V., "Three-dimensional hypersonic gas flow past slender bodies at high angles of attack," Prikl. Matemat. Mehkan. **24,** no. 2, 205–212 (1960).

8 Bloom, M. H. and Steiger, M. H., "Inviscid flow with nonequilibrium molecular dissociation for pressure distribution encountered in hypersonic flight," J. Aero/Space Sci. **27,** 821–835 (1960).

9 Whalen, R. J., "Viscous and inviscid nonequilibrium gas flows," Inst. Aerospace Sci. Preprint 61-23 (January 1961).

10 Vaglio-Laurin, R. and Bloom, M. H., "Chemical effects in external hypersonic flows," ARS Preprint 1976-61 (August 1961).

11 Hall, J. G., Eschenroeder, A. Q., and Marrone, P. V., "Inviscid hypersonic air-flows with coupled nonequilibrium processes," Inst. Aerospace Sci. Preprint 62-67 (January 1962).

12 Capieux, R. and Washington, M., "Nonequilibrium flow past a wedge," Inst. Aerospace Sci. Preprint 62-99 (June 1962).

13 Teare, J. D., Hamerling, P., and Kivel, B., "Theory of the shock front, high temperature reaction rates," Avco Research Lab. Research Note 133 (June 1959).

14 Camac, M., "O_2 vibration relaxation in oxygen-argon mixtures," J. Chem. Phys. **34,** 448–459 (1961).

15 Benson, S. W. and Fueno, T., "The mechanism of atom recombination by consecutive vibrational deactivations," J. Chem. Phys. **36,** 1597–1604 (1962).

16 Freeman, N. C., "Nonequilibrium flow of an ideal dissociating gas," J. Fluid Mech. **4,** Part 4, 407–425 (August 1958).

17 Bray, K. N. C., "Atomic recombination in a hypersonic wind-tunnel nozzle," J. Fluid Mech. **6,** Part 1, 1–32 (July 1959).

18 Inger, G. R., "The nonequilibrium flow behind strong shock waves in a dissociated ambient gas," Douglas Aircraft Co. Inc., Rept. SM-38936 (January 1962).

19 Inger, G. R., "Viscous and inviscid stagnation flow in a dissociated hypervelocity free stream," *Proceedings of the 1962 Heat Transfer and Fluid Mechanics Institute* (Stanford University Press, Stanford, Calif., 1962), pp. 95–108.

20 Hayes, W. D., "On hypersonic similitude," Quart. Appl. Math. **5,** no. 1, 105–106 (1947).

21 Lees, L. and Kubota, T., "Inviscid hypersonic flow over blunt-nosed slender bodies," J. Aero/Space Sci. **24,** 195–202 (1957).

22 Gibson, W. E., "Dissociation scaling for nonequilibrium blunt nose flows," ARS J. **32,** 285–287 (1962).